Derivation of Phenological Information from Remotely Sensed Imagery for Improved Regional Climate Modeling

Jing Wang[1], Nathan Moore[2], Jiaguo Qi[2]
Lijian Yang[3], Jennifer Olson[2], Nathan Torbick[4], Jianjun Ge[5]
[1]Department of Mathematics, Statistics, and Computer Science, University of Illinois at Chicago, 851 S Morgan Street, Chicago, IL 60607
[2]Department of Geography, Michigan Sate University, 673 Auditorium Road, East Lansing, MI 48824
[3]Department of Statistics and Probability, Michigan Sate University, A 413 Wells Hall, East Lansing, MI 48823
[4]Applied Geosolutions, 87 Packers Falls Road, Durham, NH 03824
[5] Department of Geography, Oklahoma State University, 337 Murray Hall, Stillwater, Oklahoma 74078

Abstract
Phenological information reflecting seasonal changes in vegetation is an important input variable in climate models such as the Regional Atmospheric Modeling System (RAMS). It varies not only among different vegetation types but also with geographic locations (latitude and longitude). In the current version of RAMS, phenologies are treated as a simple sine function that is solely related to the day of year and latitude, in spite of major seasonal variability in precipitation and temperature. The sine curves of phenology are far different from the reality in many parts of the globe and, therefore, derivation of more representative phenological information would improve regional climate simulations. In this study, advanced spline techniques and remote sensing observations were used to develop a set of phenological functions for all land covers in the East Africa, and subsequently used in the RAMS model simulation analysis. The results show that the spline technique can effectively be used to characterize the phenological properties of most land cover types and the use of remotely sensed phenological information in regional climate simulations resulted in much more realistic climate conditions of the East Africa region. These spline phenologies are specifically needed for future climate projections when no remote sensing data are available.

Key Words: Confidence bands, Polynomial Spline, Regional Climate Models

1. Introduction

Many studies demonstrate the influence of land use and land cover change on local and regional climate. The Climate and Land use Interaction Project, or CLIP (http://clip.msu.edu) attempts to understand the nature and magnitude of the interactions of climate and land use/cover change across East Africa.

Phenological information reflecting the seasonal variability of vegetation is an important input variable in regional climate models such as Regional Atmosphere Simulation System (RAMS). It varies not only among different vegetation types but also with geographic locations (latitude and longitude).

Many climate models use simple functions for vegetation parameters since, to first order, the planet is warmer and wetter as you approach the equator. However, East Africa is unique in having semiarid grasslands along the equator, and drastically different surface conditions govern the radiation budget in this region. Climate models are dependent on accurate representations of the surface radiation budget to replicate atmospheric development. Thus, modeling climate for a unique area like East Africa requires a different treatment of vegetation characteristics.

RAMS version 4.4 [*Cotton et al.*, 2003], a state-of-the-art three-dimensional atmospheric model, includes a representation of vegetation called the Land-Ecosystem-Atmosphere Feedback, version 2 (LEAF-2) [*Walko et al*., 2000]. For a given land cover class, LEAF-2 provides functions for several vegetation characteristics including LAI, fractional cover, roughness length, and displacement height. Although these characteristics are interrelated, we will consider only LAI here.

Remote sensing parameterization for land surface schemes in climate models is focusing on the transformation of categorical LULC information into quantitative land surface biophysical parameters [*Pitman* 2003]. The parameters that will result from this analysis, and that will be inputs to the regional climate model, include surface albedo, fractional vegetative cover, leaf area index (both senescence and green) and above ground biomass. In this paper we will investigate the variation of LAI temporally and spatially for each land cover type.

The phenological discrepancy between the RAMS model and the remote sensing measurement given in Section 2 will show that the pre-assumed relationship is significantly different from the collected information from MODIS (Moderate Resolution Imaging Spectroradiometer).

Based on the observations of LAI from MODIS data, a polynomial spline regression is employed to fit the function of each land cover type in East Africa. The fitted curve is a piecewise polynomial smoothly joined at knots, which are the equally-spaced time points of one whole year. The estimated curve is derived from the least square procedure. In this paper, the linear spline is used for simple implementation and reliable theoretical property. The corresponding statistical theory was provided in *Huang* [2003] and *Wang and Yang* [2009].

There are two great advantages of spline regression. First,it is non-parametric, i.e. the estimation only depends on the available data without assuming any specific form of the model. Second, it has a specific expression for the estimated function. Other nonparametric regression methods such as kernel or local polynomial do not produce an overall function formula. Hence the spline function is preferred for data-driven estimation and future prediction. The estimate function of LAI relies on the time and the spatial index (latitude and longitude). We developed the function first temporally and then further investigated the spatial influence.

The research objective of this study was to derive spatially explicit phenologies for all LULC types in East Africa for improved parameterization of regional climate methods (such as RAMS). By addressing this objective, the following two questions must be addressed:

- What are the differences in LAI between the observations from MODIS censor and the simulated values from RAMS?
- Are there any significant differences among the land cover types and do they vary with geographic locations?

2. Methods

2.1 Study Area and Data Description

Interdisciplinary research is being conducted in East Africa, a region that is undergoing rapid land use change and where changes in climate would have serious consequences for people's livelihoods and requiring new coping and land use strategies.

Consequently, uncertainty in climate modeling is expected to be high, partly due to uncertainty related to the use of generic land cover parameters including their phenological functions. The CLIP project also created a new land use land cover (LULC) classification based on the best available international LULC products for the East Africa region [*Ge et al.* 2005, *Torbick et al.* 2005]. The new LULC classification [*Torbick et al.*, 2006), labeled "CLIP-cover," was used as the spatial land cover layer for which the LAI remote sensing data were extracted by LULC, or land cover type.

Two primary data sets are used to develop the phenological curves. The first is a hybrid LULC classification with 34 land cover types at 1km spatial resolution for the entire study region. The hybrid combines the strengths of Global Land Cover for the year 2000 (GLC2000) [*Mayaux et al.* 2004) and Africover [*Africover* 2002] LULC products. Assessments determined GLC2000 more accurately classified natural land cover types, while Africover more accurately classified human-managed landscapes [*Torbick et al.* 2006]. The new hybrid CLIP Cover captures these strengths geospatially for a single LULC for the study region.

The second is LAI from the MODIS instrument on the Terra satellite platform. Briefly, LAI is a description of vegetation structure and the amount of plant canopy relative to a unit on the surface. In climate models, LAI is used to represent components of energy balance equations between the surface and lower atmospheric boundaries. The MODIS LAI product used, MOD15A2 v4.0 [*Knyazikhin et al.* 1999], is available at 8-day temporal intervals at 1km spatial resolution covering the entire study region in a 2-dimensional tessellation. The data was obtained through the National Aeronautics and Space Administration (NASA) Land Processes Distribution Active Archive Center.

Data was obtained from February 2000 to December 2003 at 8-day intervals. Data preprocessing included mosaicing tiles, rescaling data values, quality control for cloud cover and fill values, and reprojecting data from Integerized Sinusoidal Projection into Lambert Azimuthal Equal Area. Using the hybrid LULC product, LAI data was subset into tables by LULC type. Each table contains 8-day LAI from February 2000 – December 2003 by LULC type with geographic coordinates (latitude / longitude) at each pixel (or LAI value) representing spatial location information.

2.2 Polynomial Spline Regression

The dependence of LAI on time is investigated in the framework of nonparametric regression. To introduce this concept, let $\{(T_i, Y_i)\}_{i=1}^{n}$ be identically and independently distributed observations, satisfying

$$Y_i = m(T_i) + \sigma(T_i)\varepsilon_i, i = 1,\ldots,n,$$

where the errors ε_i have mean zero and variance one. The mean function $m(t)$ and standard deviation function $\sigma(t)$ are not assumed to be of any specific form but have to be estimated from the data directly, see *Wang and Yang* [2009]. If the data actually follows a polynomial regression model, the function $m(t)$ is a polynomial of t and $\sigma(t)$ will typically be a constant.

To introduce the concept of spline, one divides the finite interval $[a,b]$ into $(N+1)$ subintervals $J_j = [t_j, t_{j+1}), j = 0,\ldots,N-1, J_N = [t_N, b]$. A sequence of equally-spaced points $\{t_j\}_{j=1}^N$, called interior knots, are given as

$$t_0 = a < t_1 < \cdots < t_N < b = t_{N+1}, t_j = a + jh, j = 0,1,\cdots,N+1,$$

In which $h = (b-a)/(N+1)$ is the subinterval length. We approximate the mean function $m(t)$ by linear spline. These are piecewise linear functions, linear on each J_j and continuous on the entire interval $[a,b]$. The linear spline estimator of $m(t)$ based on data $\{(T_i, Y_i)\}_{i=1}^n$ is given by

$$\hat{m}(t) = \hat{a}_0 + \sum_{j=1}^{N} \hat{a}_k \cdot (t - t_j)_+ + \hat{a}_{N+1} t, \qquad (1)$$

where the coefficient are the solutions of the following least square problem

$$\{\hat{a}_0, \hat{a}_1, \ldots, \hat{a}_{N+1}\}^T = \underset{\{a_0,a_1,\ldots,a_{N+1}\}\in R^{N+2}}{\arg\min} \sum_{i=1}^{n} \left\{ Y_i - a_0 - \sum_{j=1}^{N} a_k \cdot (T_i - t_j)_+ - a_{N+1} t \right\}^2$$

in which $(t-t_j)_+ = \max\{0, t-t_j\}$ is a so-called "truncated linear function" with truncation at knot t_j.

2.3 Spline Fitting for LAI by LULC Type

As a first step we resample the LAI pixels within 0.1 latitude degree and 0.1 longitude degree together as one grid block—a scale suitable for most regional climate modeling approaches. In order to get the representative LAI values, the spatially averaged LAI at each grid is obtained for each available Julian day. The second step is to get the means of the same Julian days over four years. After the above two-step averages, LAI means of a whole year at each grid is available.

Based on the LAI means, the estimates following equation (1) is established after one step least squared procedure for each grid block. To avoid the non-continuity difference between the values of early January and late December, we duplicate the one-year data to create two-year data, hence $[a,b] = [0,730]$. For uniformity across various LULC types and locations, we pick one knot every two months, i.e. $N = 11$

$$LAI(t) = \hat{a}_0 + \sum_{j=1}^{11} \hat{a}_k \cdot (t - t_j)_+ + \hat{a}_{12} t, t_j = j \times \left(\frac{365}{6}\right), j = 1,...,11.$$

(2)

Let Z = LAI, x = latitude, y = longitude, t = Julian day. For each LC type we develop the LAI function as follows,

$$Z(x,y,t) = \hat{a}_0(x,y) + \sum_{j=1}^{11} \hat{a}_j(x,y) \cdot (t - t_j)_+ + \hat{a}_{12}(x,y) \cdot t \,,$$

(3)

The coefficients $\hat{a}_j(x,y)$ for $j = 0,1,...,12$, will be estimated based on the MODIS data at each individual grid block. The coefficients for different land cover types are listed in Tables 1 to 4.

3. Results

3.1 Land Cover Phenologies

In order to show the magnitude of the difference driven by the spatial affect, in particular the latitude, the linear spline curves estimated by formula (1), the RAMS simulation curve and the difference curve are provided at equator, 5º north, , and 5º south respectively. Each grid block covers the area of 0.1 by 0.1 degrees, the longitudinal of three grid blocks are chosen to be as close as possible. In Figure 1 of the Appendix, the green solid line represents the LAI at 5º N, the red dashed line for the equator, and the blue dotted line for 5º S.

Figure 1 illustrates several examples of the seasonal variation in LAI for common classes in the study area. The first column gives the trigonometric curve of LAI over time for four land cover types: *deciduous woodland*, *deciduous shrubland with sparse trees*, *open to very open trees*, and *rainfed herbaceous crop*. Although the length of vertical axis of the RAMS curves is the same for all four land cover types—that is, they are all 0.2— the start points of the range are slightly different. In the figures of the linear splines the range of the vertical is 6, from 0 to 6, which is a substantial difference from the RAMS default values. If the same scale is chosen, no visible variation occurs among the RAMS curve at the three latitudes. There is no longitude effect in the default RAMS values since it plays an unnoticeable role in seasonality of the model system. In addition, there is only one valley for each of the northern latitudes and one peak for each south latitudes in RAMS, and the valley or peak point is in the exact middle of the year. At the equator it always flat at any time interval no matter what land cover type is represented, in clear contradiction of East Africa's well-known dual rainy seasons.

Compared with default RAMS values, the second column in Figure 1 show that the linear spline smoothing captures the changing seasonal signals of the LAI and varying spatial effect cross the study region. Due to its data-driven attributions, splines have a better fit spatially and temporally. The green solid line (5º N) achieves its peak point of LAI around August, while all the blue dotted lines (5º S) show the largest LAI value in the spring, such as April for Deciduous Woodland. The fact is not surprising that the northern and southern curves are symmetric about the center, June, for each type because the two locations are symmetric about the equator. For all four land cover types, the LAI at the equator has greater LAI than those far away from the equator. Especially for land cover type *rainfed herbaceous crop*, the regression line at the equator is far above both spline regression lines at 5ºN and 5ºS latitude. The linear spline estimates produce two noticeable valleys at the equator. That is a big difference from the constant LAI value of RAMS. The LAI varies at the equator over time; it is not fixed given the distinct bimodal weather pattern.

The last column in Figure 1 shows the differences between the LAI values from default RAMS values and the linear spline estimates. This is evident from the graph, except there is little overlap between the difference at equator and the "0 line" for land cover types; the remaining distance is very large. The statistical testing of the differences is given in next section.

In summary, the observed LAI and resultant splines are distinctly different from the RAMS/LEAF-2 default parameterization, with the LEAF-2 parameterization completely failing to capture the seasonality at the equator or in the regions +/- 5° away. The spline parameterizations accurately capture bimodal greening events at the equator, unimodal features away from the equator, and the very low LAI for maize regions following harvest.

3.2 Sensitivity and Uncertainty

Confidence bands of a function estimator are the collection of simultaneous confidence intervals over the range of data. It can be used to test the hypothesized curve. Linear spline confidence bands were developed in Wang and Yang [2009]. Given a small significance level (less that 0.05), the confidence bands based on the sample information can be obtained. If the null curve is totally covered by the upper and lower confidence bands, then its deviation from the true curve is insignificant and will be accepted as a valid representation of the true curve; otherwise, it should be rejected as the null curve, since it is significantly different from the data pattern.

In this paper, the hypotheses for a given land cover type are:

Ho: LAI trend curve follows the default RAMS Curve

Ha: LAI trend curve does not follow the default RAMS Curve.

For the test, the same data from the previous four land types for comparison is used. The three columns correspond to the grid point at 5º N, at equator and 5º S. The blur solid line represents the LAI value of the RAMS, the green dotted line is the linear spline regression line, and the dashed red lines (upper and lower) are the confidence bands derived from the MODIS data given the significance level 0.001.

Although tested with a significance level as low as 0.001, the RAMS curve falls totally outside of both bands for 5º N and 5º S. At the equator there is some overlap for *deciduous woodland* and *deciduous shrubland with sparse trees*; however, it is still far from being totally covered by the bands. Therefore this test illustrates that the RAMS curves overestimate the LAI, with the difference being significantly large indicated from the small p-value <0.001.

3.3 Phenological Functions of Land Cover

To model the LAI spatially, the coefficients $\hat{a}_j(x, y),\ j = 0,..,12$ in equation (3) are further approximated with quadratic functions of *x* and *y*. The same four dominant land cover types are selected for analysis.

From Section 2, a coefficient set with 13 coefficient elements $\{\hat{a}_j(x, y),\ j = 0,1,..,12\}$ is obtained. Each coefficient element $\hat{a}_j(x, y)$ is related to all grid points. For better regression, the outliers (grid points) are first detected and removed from the coefficients based on the screening of the kernel density estimators. Then the corresponding part in

the data set will be left out too. The deleted outliers are shown in the next table. At most 5.4% out of the whole data will not affect the regression.

Outliers	Deciduous with Shrubland Trees	Deciduous Woodland	Open to Very Open Trees	Rainfed Herbaceous Crop
Grid points (%)	348 (4.831%)	344 (3.985%)	269 (5.418%)	324 (5.234%)
Data points (%)	16254 (3.2%)	16084 (2.672%)	14334 (3.982%)	18448 (4.068%)

The polynomial regression is applied to fit the above trimmed coefficients. The employed function is as follows for $j = 0,1,...,12$

$$\hat{a}_j(x, y) = c_0 + c_1 x + c_2 x^2 + d_1 y + d_2 y^2 + e_1 xy \,. \quad (4)$$

By the ordinary least square procedure, the new set of coefficients $(c_0, c_1, c_2, d_1, d_2, e_1)$ are obtained for the previous four land cover types and are listed in Table 1 to Table 4 in Appendix.

Employing the table coefficients for $\hat{a}_j(x, y)$ in (4), and further plugging into equation (3), the LAI estimates are obtained based on the parametric regression spatially and spline regression temporally. There is negligible amount of unreasonable estimates.

LAI Estimates	Deciduous with Shrubland Trees	Deciduous Woodland	Open to Very Open Trees	Rainfed Herbaceous Crop
Less than 0	699 (0.142%)	369 (0.062%)	122 (0.035%)	110 (0.025%)
Between 0 and 7	99.858%	99.938%	99.965%	99.975%

When we replace all the negatives with 0, then the linear correlation coefficients between the final estimates and the raw LAI is provided in the following table.

	Deciduous with Shrubland Trees	Deciduous Woodland	Open to Very Open Trees	Rainfed Herbaceous Crop
Linear Correlation Coefficient	0.62814	0.57409	0.59555	0.53253

3.4 Example from Application in RAMS

Figure 3 shows LAI values at 8 May 2000 for three combinations of land cover and LAI phenology, along with a MODIS image for comparison. LAI exerts a strong influence on the radiation budget at the surface, and when incorporated into models it can improve accuracy [Lu and Shuttleworth 2002]. Figure 2(a) shows grid-cell-averaged LAI for OGE with LAI values assigned from LEAF-2. Figure 2(b) shows CLIPCover re-assigned or "crosswalked" with the same vegetation classes in the LEAF-2 lookup table. Figure 2(c) shows the LAI distribution using the CLIPCover classes, but with LAI values assigned based on the MODIS-derived spline functions. Here, class-specific time curves

of LAI (splines) have been estimated for different regions to generate look-up tables for LAI more appropriate for these regions than LEAF-2. Figure 2(d) shows the raw MODIS LAI for the date selected. Since RAMS treats LAI slightly differently from MODIS, the example shown here has been corrected for this discrepancy. The profound difference in LAI from 2(a) to 2(d) at the Equator shows that the LEAF-2 function is essentially treating the semidesert of eastern Kenya as having high LAI with no variation. These successive improvements have helped to give a more precise surface parameterization while keeping the flexibility needed to accommodate projected land use change.

4. Discussion

4.1 Complexity of Land Cover Types

The imagery data for each land cover type is collected from January 2000 to December 2003, roughly every 8 days for each pixel (solution = 1 kilometer). Some difficulties that have been encountered were empty cells due to cloud cover, particularly in the eastern forested areas, and the small size and complex characterizations of some land covers. An inherent mismatch exists between plot scales (at the size of trees) and the regional climate modeling scale (in this case, about 36 km). For the purpose of this application, anything smaller than mesoscale circulations could not be adequately characterized in the model, and thus the spline functions could be applied under the assumption that the lower atmosphere is well mixed at sub-grid scale resolutions. The averaging within a climate model grid presumes that land cover classifications in one area are very similar to those of another, which may not be true for areas with extremely different seasonality. While climate models would be easier to run without the use of land cover classes – instead using directly input albedo and so forth from remote sensing— future projections of climate that include LULC change must include some sort of land cover classification, and improvements in differentiating complex land cover types should lead to better land cover parameterizations and better climate simulations. Similar efforts at improvement (e.g. Bounoua et al. 2000 for NDVI, Houldcroft et al. 2009 for albedo,) have shown meaningful gains in GCM performance. Similar gains in performance using this approach are detailed in Moore et al. (2010).

4.2. How the Spline Model Depicts the Nature of Each Type

We calculated the mean for each grid (0.1 degree) at every available Julian day. For each specific grid, the LAI of each land cover type can be seen as a series of data points over explanatory variable time (one year). Thus, we treated each series of LAI at each grid as a univariate function of time. The polynomial spline regression was employed to get the linear spline estimator of LAI, which is shown in Figure 1.

In order to capture the spatial features of each land cover type, we combined all the regression coefficient of linear splines. Then for each coefficient we perform the polynomial regression on the spatial index, latitude and longitude. The corresponding outcomes are listed in the tables of Appendix.

4.3. Contrast to Other Phenological Approaches

In general, this approach resulted in a large improvement over the generic parameters in RAMS in the representation of seasonal variability of LAI. This improvement is expected to significantly improve the seasonal precipitation pattern and temperature in RAMS scenarios (Moore et al. 2010). For certain land cover, the phenological information varies spatially. At the same grid point the phenologies change for different land covers. An alternative solution to providing phenologies is using MODIS imagery directly, and this

is frequently used in some climate projections. However, generalizing phenological change by using the nearest available MODIS data may not be an effective solution for future projections because of land cover change. In complex terrain like East Africa, adjacent pixels of a given class (e.g. rainfed agriculture) may have significantly different seasonal responses like crop harvesting date just by virtue of being at higher altitude or in the rain shadow of a mountain. This approach thus offers a solution that is designed to be flexible with land cover change. This approach differs from the Jönsson and Eklundh (2002) approach characterized by TIMESAT in that land cover classes are not masked for.

4.4. Future Directions

Sensitivity needs to be quantified spatially and by land cover type. For better estimation and prediction, the time dependence and the spatial correlation should be considered. There are more influences like elevation, topology, and distance to other geographic features such as ocean, lakes, mountain and presence of human settlement etc. As climate model resolution increases, the demand for correspondingly accurate resolution on phenological parameterizations will also increase. An immediate near-term goal is to contrast a land-cover-masked Gaussian approach like TIMESAT with this spline parameterization and determine how the techniques differ.

Acknowledgements

This research has been funded as part of the National Science Foundation Biocomplexity of Coupled Human and Natural Systems Program, Award No. BCS-0308420 and by the Michigan State University Foundation. Also in part, this work was support by NSF grant (DMS 1107017) and NASA grant (NNG05GD49G).

References

Africover. (2002). *Africover- Eastern Africa Module. Land cover mapping based on satellite remote sensing*. Food and Agriculture Organization of the United Nations.

Cotton, W. R., and Coauthors, (2003). RAMS 2001: Current status and future directions. *Meteorology and Atmospheric Physics, 82*, 5-29. doi:10.1007/s00703-001-0584-9.

Bounoua, L., G. J. Collatz, S. O. Los, P. J. Sellers, D. A. Dazlich, C. J. Tucker, D. A. Randall, 2000: Sensitivity of Climate to Changes in NDVI. *J. Climate*, **13**, 2277–2292.

Houldcroft, Caroline J., William M. F. Grey, Mike Barnsley, Christopher M. Taylor, Sietse O. Los, Peter R. J. North, 2009: New Vegetation Albedo Parameters and Global Fields of Soil Background Albedo Derived from MODIS for Use in a Climate Model. *J. Hydrometeor*, **10**, 183–198.

Huang, J. (2003), Local asymptotics for polynomial spline regression. *The Annals of Statistics, 31*, 1600-1635.

Jonsson, P.; Eklundh, L, 2002. Seasonality extraction by function fitting to time-series of satellite sensor data. IEEE Transaction on Geoscience and Remote Sensing 40 (8), 1824 – 1832.

Knyazikhin, Y., J. Glassy, J. L. Privette, Y. Tian, A. Lotsch, Y. Zhang, Y. Wang, J. T. Morisette, P.Votava, R.B. Myneni, R. R. Nemani, S. W. Running, (1999) MODIS Leaf Area Index (LAI) and Fraction of Photosynthetically Active Radiation Absorbed by Vegetation (FPAR) Product (MOD15) Algorithm Theoretical Basis Document, http://eospso.gsfc.nasa.gov/atbd/modistables.html.

Mayaux, P. Bartholome, E., Frtiz, S. and Belward, A. (2004). A new land-cover map of Africa for the year 2000. *Journal of Biogeography, 31*, 861-877.

Moore N , N Torbick, B Pijanowski, B Lofgren, J Wang, D-Y Kim, J Andresen, J Olson, 2010. Adapting MODIS-derived LAI and fractional cover into the RAMS model for East Africa, Int. J. Climatol., 30 (13), 1954–1969.

Olson, J. M., Alagarswamy, G. , Andresen, J., Campbell, D.J., Ge, J., Huebner, M., Brent Lofgren, B., Lusch, D.P., Moore, N., Pijanowski, B.C., Qi, J., Torbick, N., Wang, J. and Yang, L. (2008) Integrating diverse methods to understand climate-land interactions at multiple spatial and temporal scales, GeoForum, 39, 898-911.

Pitman, A., (2003). The evolution of, and revolution in, land surface schemes designed for climate models. *International Journal of Climatology, 23*, 479-510.

Torbick, J., Qi, J., Ge, J., D., Olson, N. Lusch,. (2005) An Assessment of Africover and GLC2000 using general agreement and airborne videography. *Geoscience and Remote Sensing Symposium, 2005 IGARSS'05. Proceedings 2005 IEEE International*, 7, 5005–5008 .

Torbick, N. Qi, J., Lusch, D., Olson, J., Moore, N., Ge, J. (2006) Developing land use land cover parameterization for climate-land modelling in East Africa. *International Journal of Remote Sensing, 27,* 4227-4244.

Walko, R.L., Band, L.E., Baron, J., Kittel, T.G.F., Lammers, R., Lee, T.J., Ojima, D., Pielke Sr., R.A., Taylor, C., Tague, C., Tremback, C.J., Vidale, P.L., 2000. Coupled atmosphere – biophysics – hydrology models for environment modeling. *Journal of Applied Meteorology 39*, 931– 944.

Wang, J. and Yang, L. (2009), Polynomial Spline Confidence Bands for Regression Curves. Statistica Sinica, 19, 325 --342.

Appendix

Table 1. Coefficients Table for Land Cover Type - Deciduous Shrubland with Sparse Trees						
	c_0	c_1	c_2	d_1	d_2	e_1
$\hat{a}_0$	13.86733	0.189258	-0.01538	-0.61737	0.007717	-0.00977
$\hat{a}_1$	0.501879	0.009621	0.000144	-0.02756	0.00039	-0.00021
$\hat{a}_2$	-0.63643	-0.00351	-1.1E-05	0.033409	-0.00044	0.000168
$\hat{a}_3$	0.425755	-0.00089	-7.2E-05	-0.02161	0.000266	-1.6E-05
$\hat{a}_4$	0.230287	-0.00537	-0.00025	-0.01455	0.000229	0.000037
$\hat{a}_5$	-0.38993	0.001671	-7.7E-05	0.022872	-0.00033	-6.9E-05
$\hat{a}_6$	-0.17788	-6.9E-05	0.000194	0.010029	-0.00015	0.000025
$\hat{a}_7$	0.560264	0.007802	0.000233	-0.03082	0.000431	-0.00013
$\hat{a}_8$	-0.65163	-0.00305	-3.8E-05	0.034248	-0.00045	0.000146
$\hat{a}_9$	0.430822	-0.00104	-6.2E-05	-0.02189	0.00027	-8E-06
$\hat{a}_{10}$	0.222698	-0.00512	-0.00026	-0.01413	0.000224	0.000024
$\hat{a}_{11}$	-0.36273	0.000745	-1.7E-05	0.021394	-0.00031	-2.3E-05
$\hat{a}_{12}$	-0.2125	-0.00392	0.000027	0.012197	-0.00018	0.00008

Table 2. Coefficients Table for Land Cover Type - Deciduous Woodland.						
	c_0	c_1	c_2	d_1	d_2	e_1
$\hat{a}_0$	15.60422	0.258968	-0.01681	-0.7006	0.008762	-0.01201
$\hat{a}_1$	0.285465	0.010554	0.000218	-0.01437	0.000196	-0.00021
$\hat{a}_2$	-0.52319	-0.00485	-3.6E-05	0.025799	-0.00032	0.000184
$\hat{a}_3$	0.423792	-0.00264	-0.00014	-0.02168	0.000263	0.000014
$\hat{a}_4$	0.165587	-0.00551	-0.00016	-0.01029	0.000164	0.000077
$\hat{a}_5$	-0.44096	0.003254	-0.00018	0.025446	-0.00036	-0.00014
$\hat{a}_6$	0.062666	0.000927	0.000261	-0.00331	0.000032	0.00001
$\hat{a}_7$	0.322273	0.008389	0.000262	-0.01656	0.000226	-0.00012
$\hat{a}_8$	-0.53571	-0.00429	-4.9E-05	0.026532	-0.00033	0.000161
$\hat{a}_9$	0.428083	-0.00285	-0.00013	-0.02193	0.000267	0.000022
$\hat{a}_{10}$	0.157467	-0.0052	-0.00017	-0.00982	0.000158	0.000064
$\hat{a}_{11}$	-0.41156	0.002126	-0.00014	0.023738	-0.00034	-9.7E-05
$\hat{a}_{12}$	-0.07965	-0.00318	-1E-06	0.004623	-7.5E-05	0.00005

Table 3. Coefficients Table for Land Cover Type - Open to Very Open Trees.

	c_0	c_1	c_2	d_1	d_2	e_1
$\hat{a}_0$	21.36797	0.582205	-0.01761	-0.9429	0.011065	-0.01953
$\hat{a}_1$	0.755761	0.026441	0.000046	-0.0398	0.00054	-0.00064
$\hat{a}_2$	-0.40319	-0.00305	-0.00016	0.020365	-0.00027	0.000065
$\hat{a}_3$	-0.52959	-0.02078	-1.5E-05	0.030611	-0.00044	0.000568
$\hat{a}_4$	0.583969	0.007367	-0.00017	-0.03334	0.000476	-0.00027
$\hat{a}_5$	-0.20593	-0.00388	-0.00013	0.012463	-0.00018	0.000071
$\hat{a}_6$	-0.4363	-0.00384	0.000293	0.024033	-0.00035	0.000095
$\hat{a}_7$	1.062424	0.023523	0.000225	-0.05847	0.000819	-0.0005
$\hat{a}_8$	-0.49433	-0.00221	-0.00021	0.025909	-0.00035	0.000024
$\hat{a}_9$	-0.49496	-0.02111	0.000005	0.028505	-0.00041	0.000584
$\hat{a}_{10}$	0.529546	0.007892	-0.00021	-0.03003	0.000427	-0.0003
$\hat{a}_{11}$	-0.01689	-0.00576	-1.4E-05	0.000928	-8E-06	0.000164
$\hat{a}_{12}$	-0.22684	-0.01172	0.000174	0.011508	-0.00016	0.000297

Table 4. Coefficients Table for Land Cover type - Rainfed Herbaceous Crop.

	c_0	c_1	c_2	d_1	d_2	e_1
$\hat{a}_0$	27.46197	0.516892	-0.01812	-1.34425	0.017536	-0.01782
$\hat{a}_1$	0.665941	0.016663	0.000098	-0.03529	0.000488	-0.00035
$\hat{a}_2$	-0.30472	0.00122	-0.0002	0.015172	-0.0002	-7.9E-05
$\hat{a}_3$	-0.44979	-0.01913	-2E-06	0.0253	-0.00035	0.000526
$\hat{a}_4$	0.59182	0.004496	-0.00022	-0.03303	0.000461	-0.0002
$\hat{a}_5$	-0.11557	-0.00089	-0.00021	0.006697	-9.1E-05	-3.5E-05
$\hat{a}_6$	-0.56834	-0.0029	0.000415	0.031754	-0.00046	0.000102
$\hat{a}_7$	0.902208	0.017373	0.000252	-0.04916	0.000688	-0.0003
$\hat{a}_8$	-0.37557	0.001015	-0.00024	0.019326	-0.00026	-9.1E-05
$\hat{a}_9$	-0.4228	-0.01907	0.000015	0.023719	-0.00033	0.000531
$\hat{a}_{10}$	0.54799	0.004403	-0.00024	-0.03046	0.000424	-0.00021
$\hat{a}_{11}$	0.038773	-0.00055	-0.00012	-0.00236	0.000039	-5E-06
$\hat{a}_{12}$	-0.28223	-0.00642	0.000175	0.015208	-0.00022	0.000154

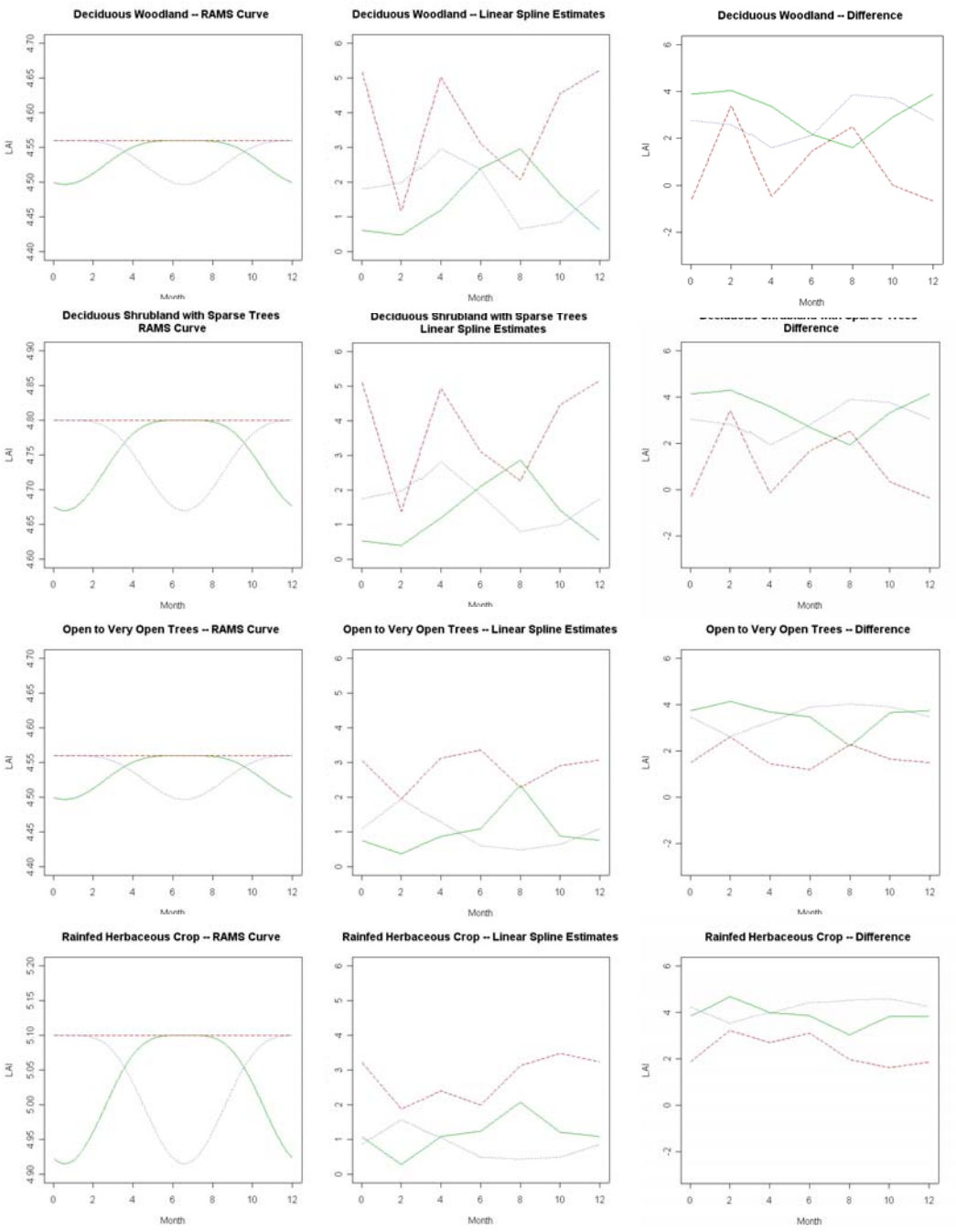

Figure 1. Comparison Between the RAMS Curve of LAI and Its Linear Spline Estimates Derived from MODIS Data.

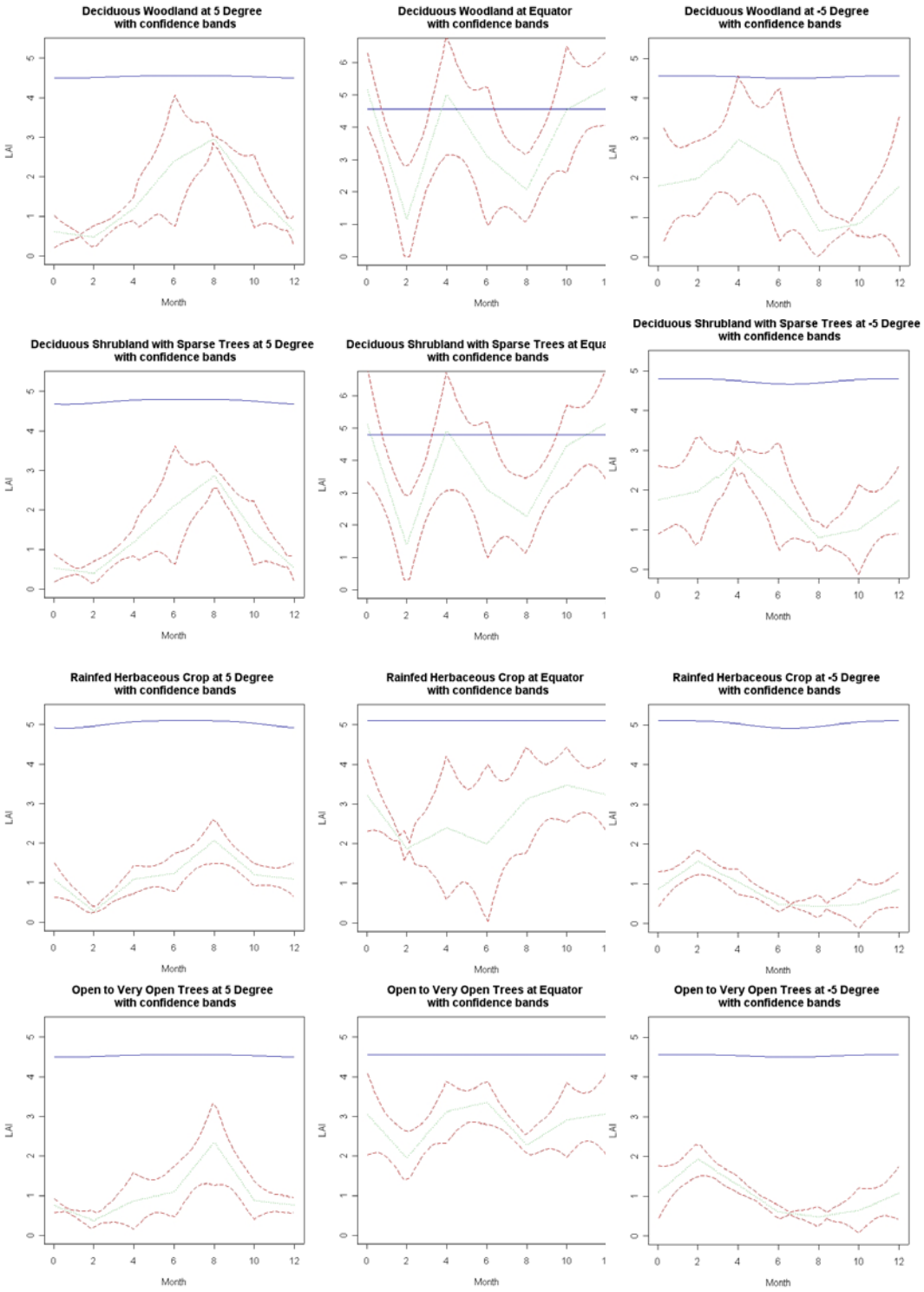

Figure 2. Confidence Bands of the Linear Spline Estimates and the RAMS Curves.

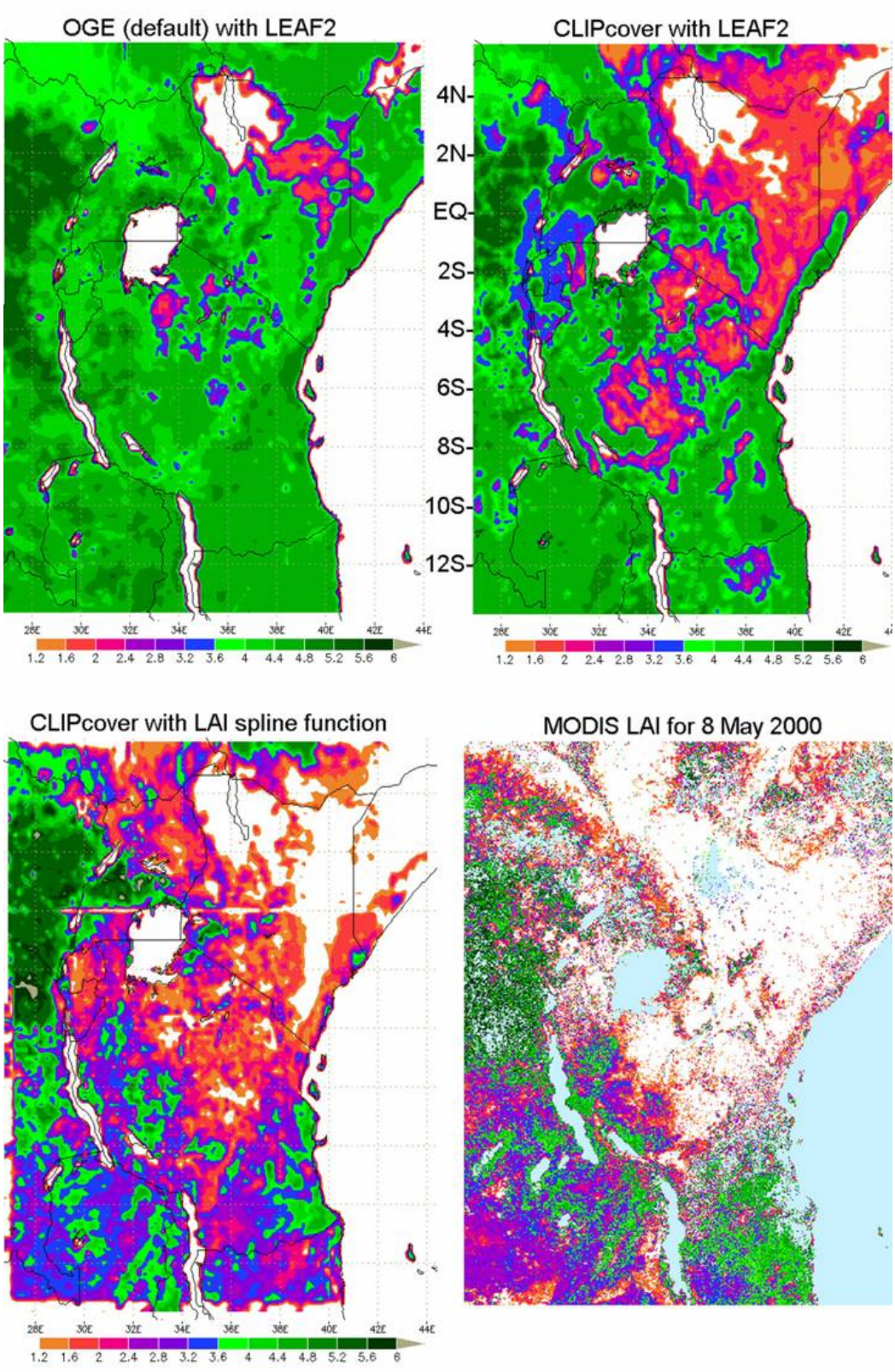

Figure 3. Improved Representation of Land Surface in RAMS.